A Two Part Research Study into Medical Technology and Drug Repurposing

Ayush Jain

General Introduction:

This research project contributes to the medical field in two ways: optimizing the radiologists' workflow using small convolutional neural networks and proving that a medicine could be used for choroidal tumor regression.

Part one of this paper is an individual research project to find the machine learning model that best-balanced size and accuracy when screening frontal chest x-ray scans. For this project, I learned Python and machine learning on my own using *Automate the Boring Stuff* to learn Python and deeplizard.com to learn machine learning.

Part two of this paper is a case study documenting that anti-VEGF Eylea successfully reduced a choroidal tumor secondary to endometrial cancer's size. This case was assigned to me when I shadowed at a retinal research facility (Wagner Macula and Retina Center) this summer. My interest in the eye was instilled in me by my dad, an ophthalmologist.

Working under retina specialist Dr. Kapil Kapoor's research team, I witnessed videos of surgery, treatment procedures being conducted on patients in other research studies, learned the finances behind a research facility, and learned more about the patient whose case study I was assigned to write.

Through this project, I got a taste of both sides of medical research and would like to combine both in college through research into the field of DNA Data Storage.

PART 1:

Screening and Prioritizing Abnormal Chest X-Rays with Small Deep Learning Algorithms

Ayush Jain

Ocean Lakes High School

Abstract

Trends predict the global shortage of physicians will continue to grow, increasing the workload burden on practicing doctors. This study experiments with popular small convolutional neural networks to screen and prioritize frontal chest x-ray scans to ease the radiologists' workflow and allow more critical patients to receive care faster. Using the model that best balances size and accuracy, I created a web application to order the scans from most likely abnormal to least likely. To my knowledge, this is the only study that focuses solely on small models for this application. Doing this with a low-latency model takes steps towards closing the medical digital divide. It strives to provide access to resources like machine learning to all who have access to a computer (even ones with poor computational capabilities). A modified MobileNetV2 model was trained on the dataset and recorded a test accuracy of 93.86%, area under the curve (AUC) of 0.94, precision of 93.86%, and recall of 92.40%. The MobileNetV2 model performed the best in balancing size and accuracy among the small models, sacrificing 1.85% accuracy compared to ResNet50, a base large model, while having 10.44x fewer parameters. These results provide a precedent for further research into applying small models to medicine to shorten the medical digital divide.

Keywords: Radiology, Deep Learning, Digital Divide

Screening and Prioritizing Abnormal Chest X-Rays with Small Deep Learning Algorithms

Ayush Jain

1. Introduction

Chest X-rays are the most common radiographs performed today in hospitals for the diagnosis of multiple diseases. Their image displays one's lungs, hearts, airways, blood vessels, and bones of the spine and chest [1]. These scans give hints to detect pneumonia, COVID-19, cardiomegaly, fractures, and cancerous masses, to name a few. Due to the severity of the outcome of an abnormality in this region, a radiologist must see the scan and provide a diagnosis promptly. However, recently, there has been a notable decline in the supply of radiologists accompanied by an increase in their demand, resulting from both the pandemic and an aging world population. An inadequate supply of radiologists results in higher workloads and thus worse working conditions and overall quality of care. Additionally, it can result in higher burnout rates: in an online survey of physicians, radiology was among the specialties with the highest reported physician burnout rate, with a rate of 46% [3]. To ease the radiologists' workflow, some have turned to deep learning.

Convolutional neural networks (CNNs), a form of deep learning, have seen success in medical image classification and segmentation, as well as for a wide variety of other computer-vision-related tasks. CNNs have two parts: feature extraction and image classification. The feature extraction portion is done by a series of convolution operations followed by non-linear activation functions to extract distinguishing features for classification. Traditional image classification models utilize separate modules to extract features and train a classifier. One critical reason for the success of CNNs is that it includes the feature extraction module in the learning process to achieve an end-to-end learning framework. The optimized features for a given task outperformed traditional features resulting from feature engineering by huge margins, making CNNs a dominant player for almost all computer vision applications [13, 15, 24].

Most studies on the application of CNNs on chest x-rays focus on a single ailment [26]; however, there have been a few studies where the goal is to classify the scans with all disorders into abnormal and normal [23]. My study falls in between, as I trained models to classify the scans

into abnormal and normal categories, but the abnormal class was only composed of diseases that result in lung opacification (ex: pneumonia).

With some hospitals not having an active radiologist due to the global physician shortage [12], screening the scans before the radiologist views them is imperative for critical patients to receive timely care. However, only a mobile phone (or a device with comparable computational abilities) is available in some of these areas, so having a small model available for screening the scans is required. My study is unique because instead of focusing on attaining the model with the highest accuracy, it focuses on finding a model that can adequately classify chest x-rays with a size (parameters) that is small enough to run on a mobile phone. More generally, small models ensure that everyone has access to this novel organizational technology, preventing the digital divide from enlarging.

Specifically, my study seeks to find a model that best balances size and accuracy. My study found that MobileNetV2, a small deep learning model, sacrificed 1.85% accuracy with 10.44x fewer parameters when compared with ResNet50, a complicated image classification model consisting of 23,589,761 parameters. Because MobileNetV2 balanced size and accuracy the best, it was selected to be deployed into a self-developed web app. The web app allows a user to upload frontal chest x-ray images that it will order from most likely abnormal to least likely. Simulations have suggested that screening the radiographs in this fashion leads to scans with abnormalities being seen sooner by a radiologist (2.7 vs. 11.2 days on average) than current practice in their institution [24].

2. Methods

2.1 Dataset

The dataset of frontal chest x-rays was obtained from the RSNA Pneumonia Detection Challenge [22]. The competition got these scans from the NIH Clinical Center's public source of frontal chest-x-rays [27] and had a group of radiologists manually label them into three categories: lung

opacification, not normal/no lung opacification, and normal. Only scans with lung opacification (abnormal) and normal labels were used for this study. Table 1 lists detailed information of the dataset used in this study, and Fig. 1 shows one example scan from each of the two categories, respectively.

Table 1. Patient Population in Database

	Training (n=11780)	Validation (n=2944)	Testing (n=3682)
No. of men (%)	6697 (56.9)	1697 (57.3)	2111 (57.3)
No. of women (%)	5083 (43.1)	1266 (42.7)	1571 (42.7)
No. of AP view (%)	6051 (51.4)	1502 (51.0)	1874 (50.9)
No. of PA view (%)	5729 (48.6)	1443 (49.0)	1808 (49.1)
No. of abnormal (%)	6124 (52.0)	1526 (51.8)	1906 (51.8)
No. of normal (%)	5656 (48.0)	1419 (48.2)	1776 (48.2)
Age, y (mean ± SD)	45.2 ± 17.0	45.0 ± 16.8	45.2 ± 16.7

n: number of patients. AP: Anteroposterior. PA: Posteroanterior Anterior. y: years.

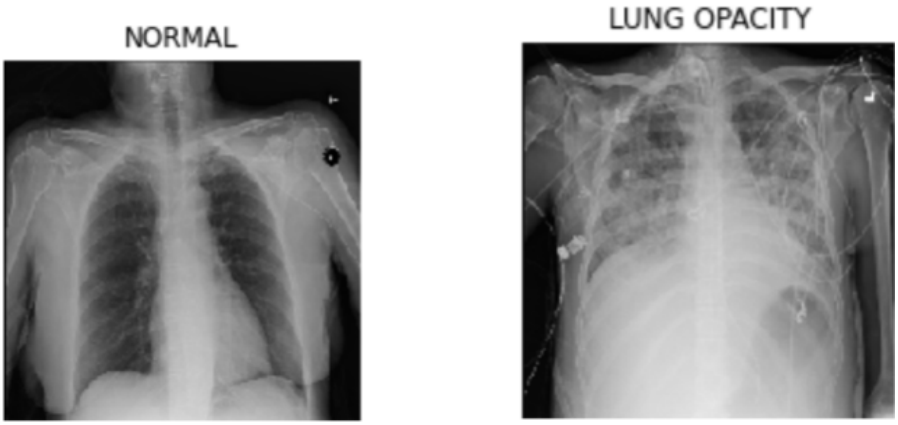

Figure 1. Example Scans. Normal vs Abnormal (Lung Opacity).

2.2 Preprocessing

The images were preprocessed in one of two ways for each model, either by rescaling each pixel to a value in the range [0,1] or using contrast limited adaptive histogram equalization (CLAHE).

The technique that resulted in higher accuracy and AUC was reported. On the training set, random data augmentation, consisting of a rotation range, zoom range, and brightness range, was performed using an image data generator (Table 2). A random seed was fixed for the iterator to ensure reproducibility. Examples of data augmentation pairs are shown in Fig. 2.

Table 2. Iterator Augmentation Parameters (Keras [6])

Iterator Augmentation Parameter	value or range
rotation_range	10
zoom_range	0.2
brightness_range	[0.8, 1.2]

No Augmentation:

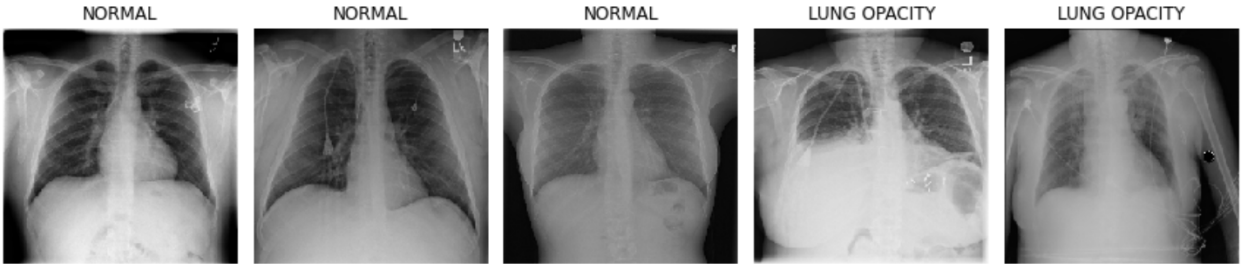

Augmentation:

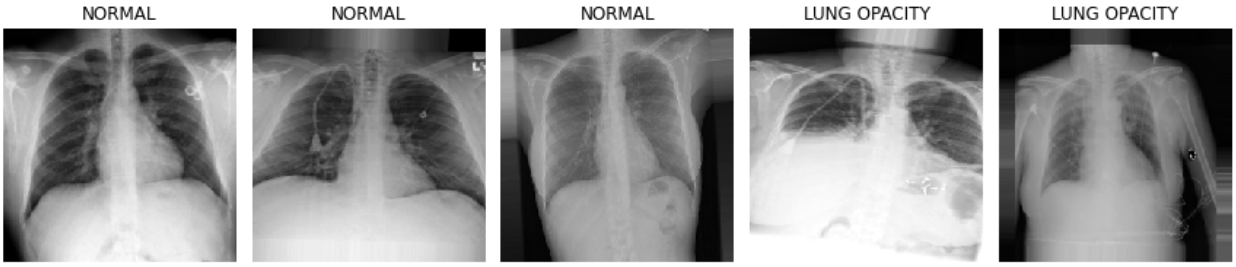

Figure 2. Examples of pairs of scans pre- (top) and post-augmentation (bottom).

2.3 Network Structures

Table 3. SepNet Architecture

Layers	Output Size	SepNet
Input	200 x 200	
Convolution	200 x 200	
Convolution	200 x 200	
Max Pooling	100 x 100	
Convolution Block - 32 filters (1)	50 x 50	(3 x 3 Separable Conv2D) x 2 Batch Normalization MaxPool2D
Convolution Block - 64 filters (2)	25 x 25	(3 x 3 Separable Conv2D) x 2 Batch Normalization MaxPool2D
Convolution Block - 128 filters (3)	12 x 12	(3 x 3 Separable Conv2D) x 2 Batch Normalization MaxPool2D Dropout (0.2)
Convolution Block - 256 filters (4)	6 x 6	(3 x 3 Separable Conv2D) x 2 Batch Normalization MaxPool2D Dropout (0.2)
Flatten	9216	
Dense block (1)	512	512D fully-connected, relu Batch Normalization Dropout (0.7)
Dense block (2)	128	128D fully-connected, relu Batch Normalization Dropout (0.5)
Dense block (3)	64	64D fully-connected, relu Batch Normalization Dropout (0.3)
Classification layer	1	1D fully-connected, sigmoid

Four models were used in this study. The first three were DenseNet121 [15], MobileNetV2 [24], and ResNet50 [13], with their last fully connected layer replaced with a single node sigmoid layer for binary classification. The fourth model, SepNet [25], was modified to test the Separable

Convolutional layers' efficiency compared to the DepthWise Separable convolution layers used in MobileNetV2. Table 3 displays the architecture of SepNet. DenseNet121, MobileNetV2, and ResNet50 are well-known models whose architectures can be found in the literature [15, 23, 13].

2.4 Performance Metrics

Accuracy, Precision, and Recall, area under a receiver operating characteristic curve (AUC) and the number of parameters in the model relative to the smallest model (MobileNetV2) were calculated on the test dataset and used to evaluate each model's performance. Some of these metrics are defined as follows,

$$\text{Accuracy} = \frac{TP + FP}{TP+FN+TN+FN} \tag{1}$$

$$\text{Precision} = \frac{TP}{TP+FP} \tag{2}$$

$$\text{Recall} = \frac{TP}{TP+FN} \tag{3}$$

where TP, FN, TN, and FN denote True Positive, False Negative, True Negative, and False Negative, respectively.

3. Experiments and Results

3.1 Experiment Setups

The images were stored in DICOM format. Each scan was resized to either (224,224) for the input to MobileNetV2, ResNet50, or DenseNet121 and (200, 200) for SepNet.

For the MobileNetV2, ResNet50, and DenseNet121 based models, to prevent overfitting, an L2 weight decay rate of 0.00001 was set for each applicable layer except the Dense output layer. These three models were trained with the ImageNet dataset, and their ImageNet-saved weights were preloaded. For these models, because the ImageNet weights were preloaded and all weights were unfrozen during training, a low learning rate of 0.00001 was used with the Adam optimizer to ensure that the model was not overcorrecting on the dataset. The fourth model, SepNet, had randomly initialized weights, so it was trained with a larger learning rate of 0.01 with the Adam optimizer.

All four models were trained for 25 epochs with a training batch size of 32. All models were implemented using the open-source Keras deep learning framework [6] and run on Google Colab [4] using a cloud GPU hardware accelerator (NVIDIA Tesla P100 16 GB).

3.2 Results

Each model was assessed using Accuracy, AUC, Precision, and Recall on the testing dataset. Table 4 displays the performance metrics for each model and Fig. 5 displays each model's confusion matrix (Fig. 5a), and receiver operating characteristic curve (ROC) from which AUC was calculated (Fig. 5b). The number of parameters (size) and accuracy relative to the smallest model (MobileNetV2) were also calculated for each model. Out of the four models, ResNet50 achieved the highest Accuracy of 95.71% and AUC of 0.958, DenseNet121 reported the best Precision of 0.983, and SepNet had the highest Recall of 0.952. SepNet was closest in parameters to MobileNetV2, only having 2.19x more parameters. MobileNetV2 only sacrificed 1.85% Accuracy and 0.017 AUC compared to the best performing model, ResNet, while having 10.44x fewer parameters.

a. SepNet:

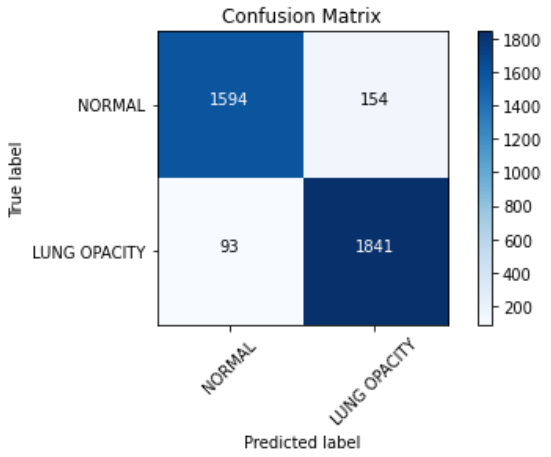

b. MobileNetV2:

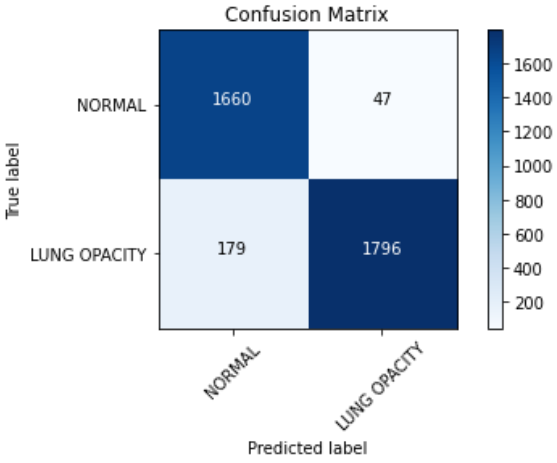

c. DenseNet121:

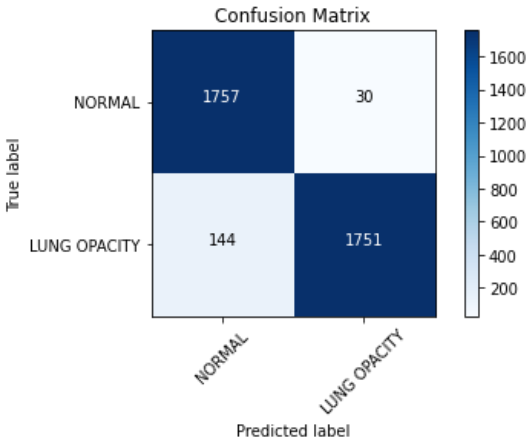

d. ResNet50:

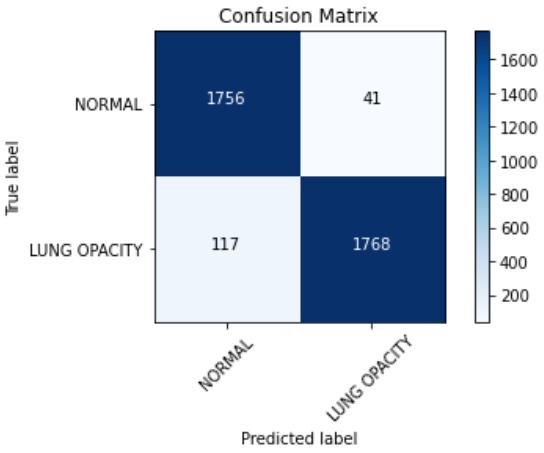

Figure 5 (a). Each Model's Test Confusion Matrix

a. SepNet:

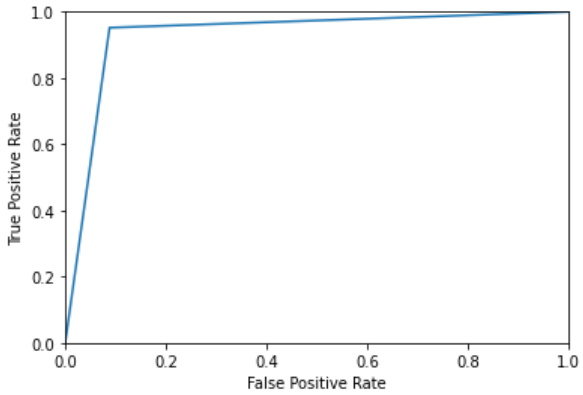

b. MobileNetV2:

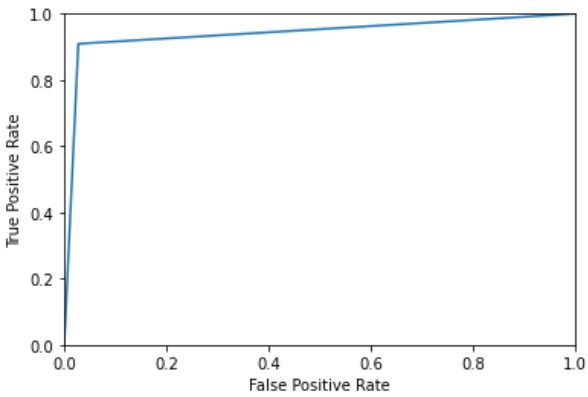

c. DenseNet121:

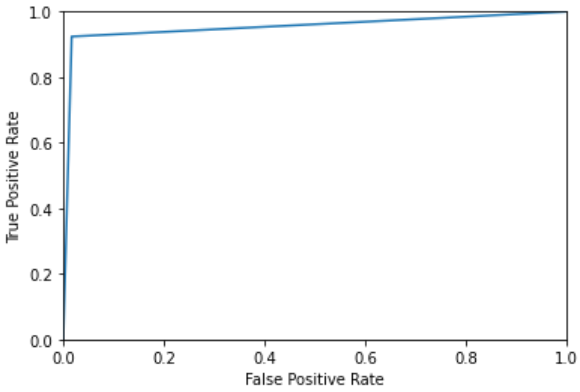

d. ResNet50:

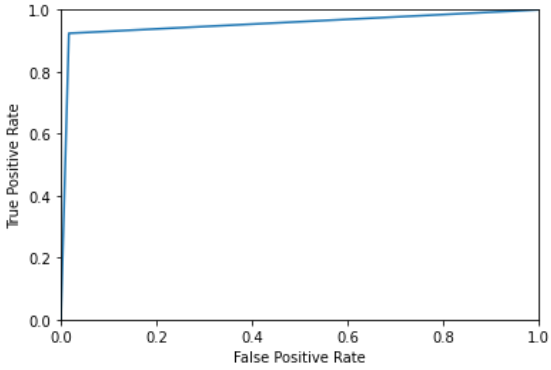

Figure 5 (b). Each Model's Test ROC Curve

Table 4: Each model's performance on the test dataset

Model	Test Accuracy (%)	Test AUC	Parameters (size)	Size compared to MobileNetV2	Test Precision	Test Recall
SepNet	93.29	0.932	4,938,593	2.19x	0.9228	0.9519
MobileNetV2	93.86	0.941	2,259,265	1.00x	0.9386	0.9240
DenseNet121	95.27	0.954	7,038,529	3.12x	0.9832	0.9240
ResNet50	95.71	0.958	23,589,761	10.44x	0.9773	0.9379

4. Model Deployment

4.1 Building the Web App

Anvil [28], a platform where users can create a web app using only Python code, was used to build an application to deploy the most efficient model. MobileNetV2 had the highest accuracy to size ratio and AUC to size ratio, so it was chosen. Users can upload scans in a batch to the model. Once uploaded, the app processes the scans as follows to predict if each of the scans is abnormal:

1. Extract and resize a pixel array from the file.
2. Run this image through the MobileNetV2 model trained to identify lung opacification.
3. Sort the images from the highest predicted probability of lung opacification to the least.
4. Display the order in a table to the user and the corresponding file name stored on the user's computer.

Fig. 6 displays the web app's input screen (Fig. 6a) and output (Fig. 6b).

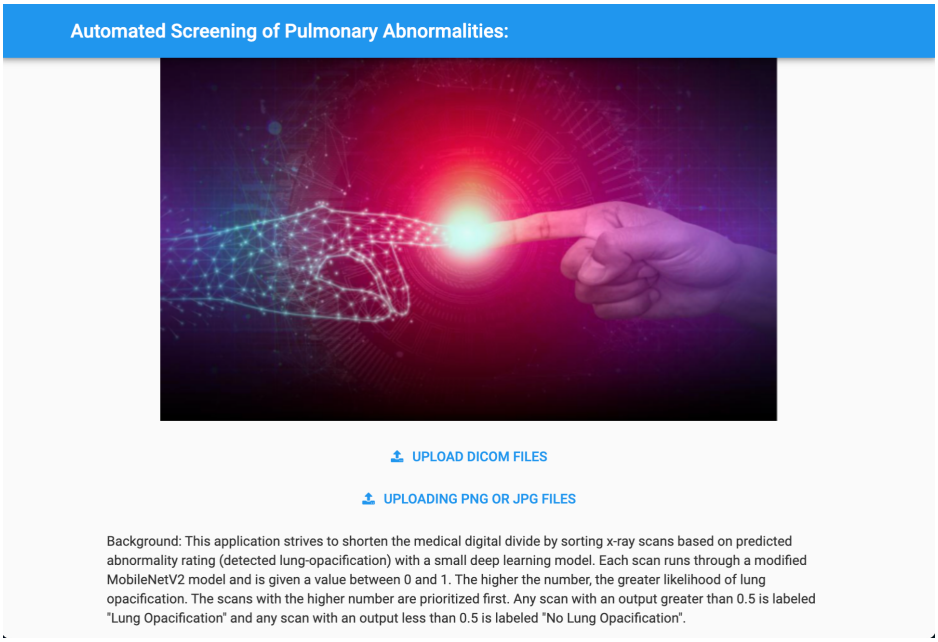

Figure 6 (a). Web App display before any input

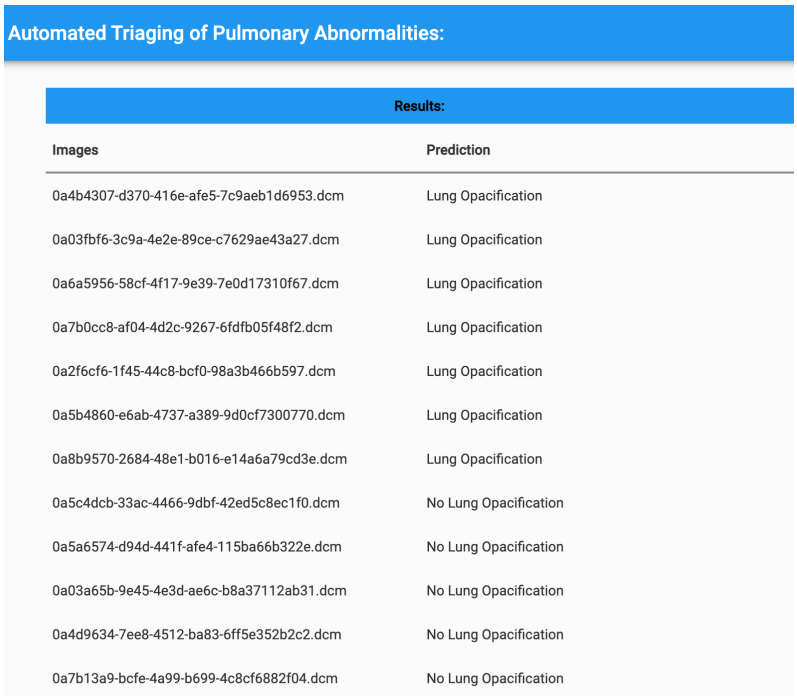

Figure 6 (b). Sample output of app after scans are uploaded

4.2 Use cases

The web app can create a more focused and organized workflow for a radiologist. By prioritizing potentially abnormal scans, patients who need the help the most are seen before less critical patients on average.

As for the medical digital divide, because of the low-latency backend (MobileNetV2), this app could run on devices with the same computational power as a mobile phone. For the web app to run, a device has to host the backend's Jupyter Notebook [19]. If the user has access to only one computer with the computational power to run the model, this computer's computational capability can be leveraged. In this case, the less-powerful devices could go to the host URL and use the app without being powerful enough to run the model, as all the computations would be done on the host computer (essentially, localized cloud computing).

5. Discussion:

Efficient screening applications in radiology are increasingly becoming important as the supply of radiologists diminishes while the demand continues to grow. This situation causes radiologists to have to cover hospitals in many different areas, causing some hospitals around the world not to have a daily radiologist available. Having an organized system of which scans are most critical to view first is invaluable in saving lives, as time is of the essence when dealing with thoracic abnormalities.

To ensure that people in most areas throughout the globe can use this application, the choice of which machine learning model to use was everything. The medical digital divide is an arising problem that will become more prevalent in radiology as more machine learning algorithms are adopted, as hospitals in developing areas may not have the technology required to run these models. Small deep learning models that produce similar results to larger models are ideal for combating these issues. This study focuses on choosing the best small model as the backend in a web application that screens and prioritizes abnormal chest x-rays to ease the radiology workflow. Also, evidence was found to suggest that models built with depthwise separable

convolutional layers are more efficient than separable convolutional layers in balancing size (parameters) and accuracy when classifying chest x-rays.

Of the varieties of base architectures, MobileNetV2 was the best balance between size and accuracy. It sacrificed only 1.8% accuracy with 10.44x fewer parameters compared with ResNet50. Additionally, MobileNetV2, trained on 11780 randomly augmented frontal chest x-rays of size (224,224), reported a test accuracy of 93.86%, precision of 97.45%, recall of 90.94%, and AUC of 0.940.

This study also supports that it is possible for images with a lot of structured noise (such as bones or devices found in the chest x-rays) to be sorted accurately by smaller models. To my knowledge, this is the first study that focuses on only small deep learning models to classify chest x-rays. Because this study is one of the few that focuses on applying small models at all. Hopefully, it can also bring attention to tackling the growing digital divide to encourage the building of more accessible machine learning technologies.

All of the dataset's labels used for training were provided by human radiologists. The two categories used in this study were scans labeled "Lung Opacification" and "Normal." Future studies could include the third category in this dataset of "Not Normal/No Lung Opacification" to see if there was a general trend that could be used to distinguish between this category and the others.

It is also important to note that the screening of the chest x-rays in order of predicted abnormality is only one use case of the model. The model could be modified for image segmentation, or it could be used as a part of an ensemble of models in a decision tree to better discern between normal and abnormal, more similar to how a human radiologist would.

6. Conclusion:

Machine learning applications can become commonplace to ease the hospital's workflow in the following decades. As the physician shortage grows, machine learning will shift from being a novelty to becoming a necessity to keep up with the rising demands of physicians from an aging population. This study presents a novel machine learning web application to screen the abnormal chest x-ray scans with a small deep learning model, making the application accessible to everyone who has a mobile phone (or a device with similar computational capabilities). The backend of this application was centered around MobileNetV2, a deep learning model that was able to classify chest x-rays with lung opacification at comparable accuracy to a model 10.44x larger (ResNet50).

1. Conflicts of Interest

This study contains no conflicts of interest.

2. Acknowledgments

My utmost gratitude goes towards Dr. Jiang Li of Old Dominion University for his advice in editing this paper.

References

[1] ACR, R. S. N. A. and. (2019, January 23). Chestrad. Radiologyinfo.org. Retrieved October 17, 2021, from https://www.radiologyinfo.org/en/info/chestrad.

[2] Allyn, J. (2019). International Radiology Societies Tackle Radiologist Shortage. Retrieved fromhttps://www.rsna.org/news/2020/february/international-radiology-societies-and-shortage.

[3] Berg, S. (2020, January 21). Physician burnout: Which medical specialties feel the most stress. American Medical Association. Retrieved October 17, 2021, from https://www.ama-assn.org/practice-management/physician-health/physician-burnout-which-medical-specialties-feel-most-stress.

[4] Bisong E. (2019) Google Colaboratory. In: Building Machine Learning and Deep Learning Models on Google Cloud Platform. Apress, Berkeley, CA. https://doi.org/10.1007/978-1-4842-4470-8_7

[5] Chang, P., Author AffiliationsFrom the Department of Radiology, AD, W., Al, E., MC, G., S, A., . . . G, C. (2018, December 11). With a Little Help from Machine Learning, Precision Radiology Can Be Feasible. Retrieved from https://pubs.rsna.org/doi/full/10.1148/radiol.2018182557.

[6] Chollet, F., & others. (2015). Keras. GitHub. Retrieved from https://github.com/fchollet/keras

[7] Choy, G., Author AffiliationsFrom the Department of Radiology, BJ, E., S, W., MI, J., M, K., Rayan, J. (2018, June 26). Current Applications and Future Impact of Machine Learning in Radiology. Retrieved from https://pubs.rsna.org/doi/full/10.1148/radiol.2018171820.

[8] Deaths: Final Data for 2015. Supplemental Tables. Tables I-21, I-22. Available from: www.cdc.gov/nchs/data/nvsr/nvsr66/nvsr6606tables.pdf

[9] Elgendi, M., Nasir, M. U., Tang, Q., Smith, D., Grenier, J.-P., Batte, C., Spieler, B., Leslie, W. D., Menon, C., Fletcher, R. R., Howard, N., Ward, R., Parker, W., & Nicolaou, S. (1AD, January 1). The effectiveness of image augmentation in deep learning networks for detecting COVID-19: A geometric transformation perspective. Frontiers. Retrieved October 8, 2021, from https://www.frontiersin.org/articles/10.3389/fmed.2021.629134/full.

[10] Franquet T. Imaging of community-acquired pneumonia. J Thorac Imaging 2018 (epub

ahead of print). PMID 30036297

[11] Gao Huang, Zhuang Liu, Laurens van der Maaten, Kilian Q. Weinberger; Proceedings of the IEEE Conference on Computer Vision and Pattern Recognition (CVPR), 2017, pp. 4700-4708

[12] Heiser, S. (2019, April 23). New Findings Confirm Predictions on Physician Shortage. Retrieved from https://www.aamc.org/news-insights/press-releases/new-findings-confirm-predictions-ph physician-shortage.

[13] He, K., Zhang, X., Ren, S. & Sun, J. Deep residual learning for image recognition. In Proceedings of the IEEE Conference on Computer Vision and Pattern Recognition 770–778 (IEEE, 2016).

[14] He, W., Zhang, Z. J., & Li, W. (2021). Information technology solutions, challenges, and suggestions for tackling the COVID-19 pandemic. International journal of information management, 57, 102287. https://doi.org/10.1016/j.ijinfomgt.2020.102287

[15] Huang, G., Liu, Z., Van Der Maaten, L. & Weinberger, K.Q. Densely connected convolutional networks. In Proceedings of the IEEE Conference on Computer Vision and Pattern Recognition 4700–4708 (IEEE, 2017).

[16] Islam, M. T., Aowal, M. A., Minhaz, A. T., & Ashraf, K. (2017, September 27). *Abnormality detection and localization in chest x-rays using deep convolutional neural networks*. arXiv.org. Retrieved October 24, 2021, from https://arxiv.org/abs/1705.09850.

[17] Kaiming He, Xiangyu Zhang, Shaoqing Ren, Jian Sun; Proceedings of the IEEE Conference on Computer Vision and Pattern Recognition (CVPR), 2016, pp. 770-778

[18] Kelly B. The Chest Radiograph. Ulster Med J 2012;81(3):143-148

[19] Kluyver, T. et al., 2016. Jupyter Notebooks – a publishing format for reproducible computational workflows. In F. Loizides & B. Schmidt, eds. Positioning and Power in Academic Publishing: Players, Agents and Agendas. pp. 87–90

[20] K. N. Akpinar, S. Genc and S. Karagol, "Chest X-Ray Abnormality Detection Based on SqueezeNet," 2020 International Conference on Electrical, Communication, and Computer Engineering (ICECCE), 2020, pp. 1-5, doi: 10.1109/ICECCE49384.2020.9179404.

[21] Lowe, David G. (1999). "Object recognition from local scale-invariant features" (PDF).

Proceedings of the International Conference on Computer Vision. 2. pp. 1150–1157

[22] Radiology Society of North America. (2018, August). RSNA Pneumonia Detection Challenge, [Version 1]. Retrieved August 28th, 2021 from https://www.kaggle.com/c/rsna-pneumonia-detection-challenge/data.

[23] Rui P, Kang K. National Ambulatory Medical Care Survey: 2015 Emergency Department Summary Tables. Table 27. Available from: www.cdc.gov/nchs/data/nhamcs/webtables/2015edwebtables.pdf

[24] Sandler, M., Howard, A., Zhu, M., Zhmoginov, A., & Chen, L.-C. (2019, March 21). MobileNetV2: Inverted residuals and linear bottlenecks. arXiv.org. Retrieved October 8, 2021, from https://arxiv.org/abs/1801.04381v4.

[25] TensorFlow Pneumonia Classification on X-rays. (2020). Chest X-Ray Images (Pneumonia), Version 6. Retrieved September 2nd, 2021 from https://www.kaggle.com/amyjang/tensorflow-pneumonia-classification-on-x-rays/notebook

[26] Tang, YX., Tang, YB., Peng, Y., *et al.* Automated abnormality classification of chest radiographs using deep convolutional neural networks. *npj Digit. Med.* 3, 70 (2020). https://doi.org/10.1038/s41746-020-0273-z

[27] Wang X, Peng Y, Lu L, Lu Z, Bagheri M, Summers RM. ChestX-ray8: Hospital-scale Chest X-ray Database and Benchmarks on Weakly-Supervised Classification and Localization of Common Thorax Diseases. IEEE CVPR 2017, http://openaccess.thecvf.com/content_cvpr_2017/papers/Wang_ChestX-ray8_Hospital-Scale_Chest_CVPR_2017_paper.pdf.

[28] Web apps with nothing but Python. Anvil. (2015). Retrieved October 28, 2021, from https://anvil.works/.

PART 2:

Regression of Choroidal Metastasis Secondary to Endometrial Adenocarcinoma from a Combination of Systemic Immunotherapy and Adjuvant Intravitreal Injections of Anti-VEGF Agents.

Ayush Jain

Ocean Lakes High School

Introduction:

To our knowledge, there are only four other cases of intraocular metastasis secondary to endometrial cancer documented in the literature. However, although metastatic endometrial cancer to the choroid is rare, it shares similar qualities with metastatic breast cancer to the choroid, the most common ocular metastasis, as they both indicate poor outcomes, with the reported cases of endometrial cancer having a lower month median survival. This case report demonstrates notable improvement of the choroidal tumor and associated subretinal fluid in the left eye as early as two weeks after the first injection of anti-vascular endothelial growth factor (anti-VEGF) concurrent with systemic immunotherapy. Augustine et al. did a literature review on the treatment of ocular metastasis with anti-VEGF, and in most cases, they found improvement with the choroidal tumor. However, their study did not contain a choroidal endometrial metastatic lesion [2].

Case Report:

A 71-year old postmenopausal female presented for a cataract evaluation with complaints of decreased vision in both eyes over two years. Her uncorrected VA was noted to be 20/150 OU, and her best-corrected VA was 20/60 OD and 20/40 OS. With glare testing done, visual acuity dropped to 20/70 OD and 20/100 OS. The dilated fundoscopic examination resulted in a cup to disk of 0.1 OU. On slit-lamp examination, there were visually significant cataracts OU with 2+ nuclear sclerosis and cortical changes. Intraocular pressures were 8 mm Hg OU; pupils were noted to be equal, round, and reactive with no afferent pupillary defect noted; visual field to confrontation was noted to be normal; ocular motility was normal. Normal vessels and periphery and normal macula and vessels were noted in the right eye.

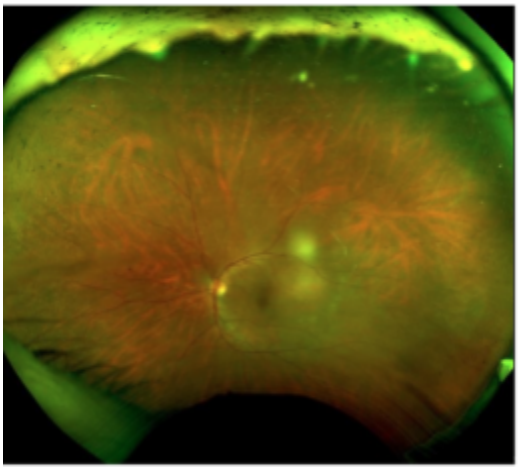

Figure 1: Fundoscopic exam (April 2021)

The left eye was remarkable for a suspicious amelanotic nevus versus melanoma in the superior temporal arcade, measuring 2.5 disc diameters with slight elevation (Figure 1).The patient’s relevant medical history was remarkable for hypertension, hypothyroidism, diabetes, and

endometrial adenocarcinoma with metastasis to the spine. The patient's retina specialist confirmed the suspicious choroidal mass was consistent with metastasis from her endometrial carcinoma. After a comprehensive discussion with the oncologist, patient, and patient's family, the joint decision was made to begin serial intravitreal aflibercept therapy to both eyes on a Q2 Week regimen parallel to her systemic immunotherapy regimen with the potential of utilizing brachytherapy if the disease was recalcitrant.

The patient continued this Q2 week regimen consistently for two months. There was a notable improvement in the choroidal tumor and associated subretinal fluid in the left eye two weeks after the first injection. The patient died from complications of metastatic endometrial cancer before beginning the third month of treatment.

Discussion:

While being the most common cancer in women, endometrial cancer rarely results in choroidal metastasis [3]. Traditionally, choroidal metastasis is treated with external beam radiation, but there are documented regression in case studies where anti-VEGF therapy is implemented. Enucleation is another treatment option for choroidal tumors; however, vision-saving methods have been preferred in recent years.

Anti-VEGF therapies have anti-angiogenesis properties targeted at tumors. This is the first case study reporting regression when the source is endometrial cancer. However, there are cases of choroidal metastasis receding from breast cancer, the largest source of choroidal tumors. Augustine et al. conducted a literature review in which they reported four previous case reports of choroidal metastasis secondary to breast cancer treated with bevacizumab, and most reported improved SRF or regression of the tumor. In this study, we found similar results with aflibercept rather than bevacizumab [2].

Lai et al. also reported using bevacizumab to treat choroidal metastasis secondary to lung cancer and reported improvement in VA in 2 weeks [7]. You et al. also found bevacizumab as an effective way to increase VA when used after systemic chemotherapy and when the metastasis was secondary to colorectal cancer [11].

Augustine et al. 's literature review concluded that there was sufficient evidence that regardless of primary cancer and site of ocular metastasis, anti-VEGF appears to improve VA, and our findings support this holds when the source is endometrial cancer [2].

The optimal dose of anti-VEGF for ocular metastasis is one of many uncertainties surrounding the treatment, with others being the intervals between treatments, number of injections, the

indications of use, and maintenance therapy. Aflibercept is a soluble decoy receptor that performs better than the body's receptors. Traditionally, it is used to treat wet AMD, but we report an effective case in treating choroidal metastasis secondary to endometrial cancer. Aflibercept and bevacizumab treatments are easy to administer and have a minimal time commitment. Additionally, it allows the patient to be out of a medical setting more than radiation therapy.

Conclusion:

This article presents a case report on the use of anti-VEGF treatment for ocular metastasis from an endometrial source. It demonstrates that anti-VEGF is an effective, non-invasive, and vision-saving treatment for ocular metastasis to improve outcomes such as tumor size and SRF.

This case study presents a 71-year-old patient effectively treated with bevacizumab in parallel to systemic immunotherapy for a choroidal tumor secondary to metastatic endometrial cancer. Similar to the current literature, this case supports adjuvant anti-VEGF injections for choroidal tumors resulting from metastatic cancers.

References:

[1] American Cancer Society. (n.d.). *Endometrial Cancer*. cancer.org. https://www.cancer.org/content/dam/CRC/PDF/Public/8609.00.pdf.

[2] Augustine, H., Monro, M., Adatia, F., Webster, M., & Fielden, M. (2014). Treatment of ocular metastasis with anti-VEGF: A literature review and case report. *CAN J OPTHALMOL*, *49*(5), 458–463.

[3] Bashshur ZF, Haddad ZA, Schakal A, Jaafar RF, Saab M, Noureddin BN. Intravitreal bevacizumab for treatment of neo- vascular age-related macular degeneration: a one-year prospective study. Am J Ophthalmol. 2008;145:249-56.

[4] Chen CJ, McCoy AN, Brahmer J, Handa JT. Emerging treatments for choroidal metastases. Surv Ophthalmol. 2011;56(6):511–521. doi:10.1016/j.survophthal.2011.05.001

[5] Cormio, G., Marino, R., Loizzi, V., Resta, L., Selvaggi, L., 2006. A rare case of choroidal metastasis presented after conservative management of endometrial cancer. Int. J. Gynecol.Cancer 16 (6), 2044–2048.

[6] Lawrence, S.D., Netland, P.A., Morris, W.R., Smiley, L., Wilson, M.W., 2010. Uterine papillary serous carcinoma metastatic to the choroid. Retin. Cases Brief Rep. 4 (1), 62–64.

[7] Makabe, K., Kurishima, K., Shiozawa, T., Miyazaki, K., Ohara, G., Kagohashi, K., Satoh, H., & Hizawa, N. (2016). Treatment of choroid metastasis from lung adenocarcinoma with bevacizumab-containing chemotherapy: A case report. *Experimental and therapeutic medicine*, *11*(1), 239–242. https://doi.org/10.3892/etm.2015.2893

[8] Saxena S, Jain A, Ramindar Sharma S*, et al*Three-dimensional spectral domain optical coherence tomography of retina in choroidal metastasis due to uterine endometrial carcinoma*Case Reports* 2012;2012**:**bcr2012006599.

[9] Smith, S. H., Arudra, S. K. C., Mullen, M. M., Palisoul, M., Dahiya, S., Kumar Rao, P., & Thaker, P. H. (2018, January 4). *A rare case of endometrial cancer metastatic to the uveal choroid*. Gynecologic oncology reports. https://www.ncbi.nlm.nih.gov/pmc/articles/PMC5760249/.

[10] Stages of uterine (endometrial) cancer. Memorial Sloan Kettering Cancer Center. (n.d.). https://www.mskcc.org/cancer-care/types/uterine-endometrial/diagnosis/stages.

[11] You, X. H., Wen, C., Xia, Z. J., Sun, F., Li, Y., Wang, W., Fang, Z., Chen, Q. G., Zhang, L., Jiang, Y. H., Wang, X. Z., Ying, H. Q., & Zong, Z. (2019). Primary Tumor Sidedness Predicts Bevacizumab Benefit in Metastatic Colorectal Cancer Patients. *Frontiers in oncology*, *9*, 723. https://doi.org/10.3389/fonc.2019.00723